Nanoscale

ROYAL SOCIETY OF CHEMISTRY

MINIREVIEW

View Article Online
View Journal | View Issue

Check for updates

Cite this: *Nanoscale*, 2022, **14**, 1123

Circularly polarized luminescent porous crystalline nanomaterials

Anyi Zheng,[a,b] Tonghan Zhao,[a,b] Xue Jin,*[a] Wangen Miao [c] and Pengfei Duan *[a,b]

Received 26th October 2021,
Accepted 23rd December 2021

DOI: 10.1039/d1nr07069j

rsc.li/nanoscale

Circularly polarized luminescence (CPL)-active materials have attracted exclusive attention because of their wide potential applications in low-power-consumption displays, encrypted information storage, chiroptical sensors, and so on. However, there is always a trade-off between the luminescence dissymmetry factor (g_{lum}) and luminescence quantum yield, which are two critical parameters. Therefore, developing materials with both large g_{lum} values and high luminescence efficiency is a key issue for constructing high-efficiency CPL materials. To date, chiral porous crystalline nanomaterials (PCNMs) including metal–organic frameworks (MOFs), porous organic-cages (POCs), metal–organic cages (MOCs), and supramolecular organic frameworks (SOFs), have shown excellent potential for solving this problem and achieving functional CPL-active materials. In this review, we will summarize several approaches for fabricating CPL-active PCNMs, such as direct synthesis, chirality induction, and symmetry breaking. Furthermore, with flexibly tunable structures and comprehensive host–guest chemistry, modulation and amplification of CPL can be achieved in these PCNMs. We would like to provide insight and perspective that PCNMs can act as an efficient platform in the CPL research field.

Published on 24 Disemba 2021. Downloaded on 8/6/2024 3:24:02 PM.

1. Introduction

Chiral substances play an important role in living systems and nature, such as D-glucose as an energy donor, L-amino acids that form the basic unit of life, double-helical DNA, and biological enzymes with catalytic activity.[1–3] Besides, chiral luminescent substances, *i.e.*, those showing circularly polarized luminescence (CPL), exhibit unique properties in optoelectronic fields. CPL is the property in which materials prefer to emit left- or right-handed circularly polarized light under excitation, which reflects excited-state chirality.[4,5] Although circularly polarized light could be generated by unpolarized light passing through a linear polarizer and a quarter-wave plate, this method results in a loss of light intensity. CPL-active materials have attracted wide attention because of their potential applications in low-power-consumption displays,[6]

[a]*CAS Center for Excellence in Nanoscience, CAS Key Laboratory of Nanosystem and Hierarchical Fabrication, National Center for Nanoscience and Technology (NCNST), No. 11 ZhongGuanCun BeiYiTiao, Beijing 100190, P. R. China. E-mail: jinx@nanoctr.cn, duanpf@nanoctr.cn*
[b]*University of Chinese Academy of Sciences, Beijing 100049, P. R. China*
[c]*School of Chemistry and Chemical Engineering, Institute of Physical Chemistry, Lingnan Normal University, Zhanjiang, 524048, P. R. China*

Anyi Zheng

Anyi Zheng received her B. Sc. degree in Chemical Engineering and Technology from Zhengzhou University (ZZU). In 2019, she enrolled in a M. Sc. course at the National Center for Nanoscience and Technology (NCNST), under the supervision of Prof. Pengfei Duan. Her recent research focuses on chiral metal–organic frameworks and chiroptical nanomaterials.

Xue Jin

Xue Jin received her Ph.D. from the Institute of Chemistry, the Chinese Academy of Sciences (CAS) in 2017 under the supervision of Prof. Minghua Liu and Long Jiang. In the same year, she joined the National Center for Nanoscience and Technology (NCNST) as an assistant researcher. Her current research focuses on supramolecular chemistry, colloidal nanocrystals, and nano-chirality.

Published on 24 Disemba 2021. Downloaded on 8/6/2024 3:24:02 PM.

encrypted storage of information,[7–9] asymmetric synthesis,[10,11] chiroptical sensors,[12,13] and so on. To evaluate the degree of CPL, the dissymmetry factor (g_{lum}) is defined as:

$$g_{lum} = 2 \times \frac{I_L + I_R}{I_L + I_R} \quad (1)$$

where I_L and I_R are the intensities of left- and right-handed light, respectively.[14] The maximum value of $|g_{lum}|$ is 2; +2 represents purely left-handed CPL while −2 represents purely right-handed CPL.

Up to now, many CPL-active materials have been designed. Chiral lanthanide complexes usually exhibit relatively considerable g_{lum} values because of large magnetic transition dipole moments, while they suffer from low luminescence efficiency.[15,16] For achieving regulatable wavelength, high luminescence efficiency, and facile processability, chiral organic molecules are considered suitable candidates for CPL-active materials. Nevertheless, to covalently combine chiral moieties and luminophores, a tedious synthesis process is often indispensable. Moreover, the g_{lum} value obtained from simple organic molecules is relatively low (10^{-5}–10^{-2}).[17,18] Against these disadvantages, molecular self-assembly has been proven to be an effective method to amplify the g_{lum} value.[19–22] However, the contribution for the enhancement of CPL only from self-assembly has been its limitation (10^{-3}–10^{-1}). Chiral liquid crystals possess an overwhelming advantage in obtaining large g_{lum} values due to the selective reflection of left- and right-handed circularly polarized light, but inevitably suppress luminescence intensity.[23,24] Additionally, most systems mentioned above have the solvent phase, which restricts their practical applications in optoelectronic devices. Therefore, developing CPL-active materials with considerable g_{lum} values and luminescence efficiency in the condensed state is of significant importance.

Chiral porous crystalline nanomaterials (PCNMs), including metal–organic frameworks (MOFs), porous organic-cages (POCs), metal–organic cages (MOCs), and supramolecular organic frameworks (SOFs), have been widely investigated on account of their potential applications in asymmetric catalysis,[25–28] enantioselective recognition, separation,[29–31] and so forth.[32,33] PCNMs can be assembled with the corresponding organic and inorganic components, providing a powerful solution for precisely controlling the arrangement of building blocks.[34] Moreover, PCNMs have applications as host matrixes owing to their porosity, variable pore size, and ultrahigh surface area. Such features enable PCNMs to enhance certain properties in the solid state. For instance, ordered structures with high crystallinity can suppress the aggregation-caused quenching (ACQ) effect of luminophores. Therefore, the integration of chiral PCNMs and luminescence to fabricate highly efficient solid-state CPL-active nanomaterials can be expected.

In this review, we emphasize the fabrication of CPL-active PCNMs through direct synthesis, chirality induction or adaption, and symmetry breaking pathways (Scheme 1). The g_{lum} factors and the measurement conditions of PCNMs derived from the aforementioned three mechanisms are summarized in Table 1. The artifacts and related strategies in the measurement of CD (Circular Dichroism) and CPL in PCNMs would be mentioned. The generation, regulation, and amplification of CPL at the nanoscale will be highlighted. We discuss the current situation and perspective of CPL-active porous crystalline nanomaterials, which are expected to develop efficient, intelligently responsive, multifunctional solid-state CPL-active materials.

2. Basic understanding and measurements of CD and CPL in porous crystalline nanomaterials

Circular dichroism (CD) is the technique for investigating the chiroptical properties of materials in the ground state. The primary observation in most samples of CD spectroscopy is the molar circular dichroism ($\Delta\varepsilon$) plotted as a function of wavelength in eqn (2):

$$\Delta\varepsilon = \varepsilon_L - \varepsilon_R \quad (2)$$

ε_L and ε_R are defined as the extinction coefficients for left- and right-hand circularly polarized light, respectively. The degree of CD can be evaluated using g_{abs}, which is defined as follows:

$$g_{abs} = \frac{\Delta\varepsilon}{\varepsilon} \quad (3)$$

where ε is the average molar circular dichroism defined as follows:

$$\varepsilon = \frac{(\varepsilon_L + \varepsilon_R)}{2} \quad (4)$$

Therefore, the final definition of g_{abs} is eqn (5):

$$g_{abs} = \frac{2(\varepsilon_L - \varepsilon_R)}{(\varepsilon_L + \varepsilon_R)} \quad (5)$$

CPL spectroscopy is the emission analogue of CD spectroscopy, and it measures the difference of emission intensity between the left- (I_L) and right-handed (I_R) circularly polarized

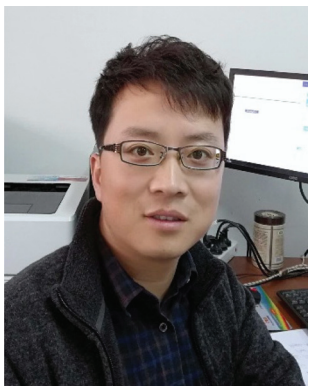

Pengfei Duan

Pengfei Duan received his Ph.D. in chemistry from the Institute of Chemistry, the Chinese Academy of Sciences (China). He worked as a postdoctoral research fellow and assistant professor at Kyushu University (Japan) from 2011 to 2015. In the end of 2015, he joined the National Center for Nanoscience and Technology (NCNST) as a full professor. His research concerns chiral nanomaterials, supramolecular chemistry, photochemistry and physics.

 This journal is © The Royal Society of Chemistry 2022

Published on 24 Disemba 2021. Downloaded on 8/6/2024 3:24:02 PM.

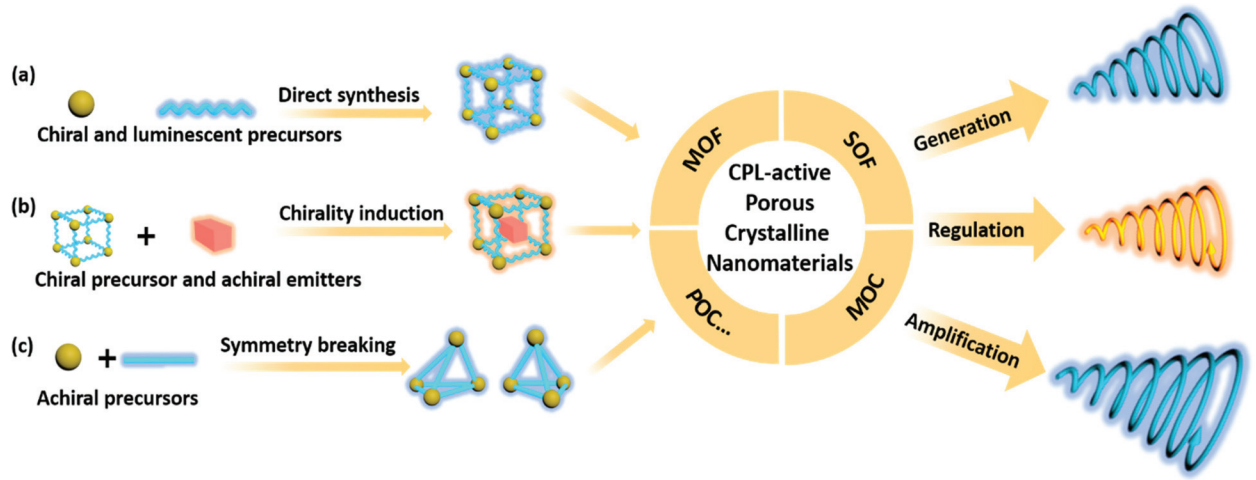

Scheme 1 Schematic illustration of trigger routes for circularly polarized luminescence of porous crystalline nanomaterials (PCNMs). Several approaches including direct synthesis, chirality induction, and symmetry breaking can fabricate CPL-active PCNMs. Owing to their structure and bonding diversity, they are flexible for regulation and amplification of CPL in these systems.

luminescence of a sample after photoexcitation with non-polarized light, and could be expressed as follows:

$$\Delta I = I_{\mathrm{L}} - I_{\mathrm{R}} \tag{6}$$

The g_{lum} factor, which qualifies the magnitude of CPL, is defined in eqn (1). Moreover, for the case of randomly oriented emission distribution, the general luminescence dissymmetry factor could be expressed as follows:[35]

$$g_{\mathrm{lum}} = 4\mathrm{Re}\left[\frac{\mu^{\mathrm{gn}} m^{\mathrm{gn}}}{|\mu^{\mathrm{gn}}|^2 + |m^{\mathrm{gn}}|^2}\right] \tag{7}$$

where μ^{gn} and m^{gn} are the electric and magnetic transition dipole moments, respectively. According to the above equation, we could figure out that a high g_{lum} factor can be obtained when the transition is electric dipole forbidden and magnetic dipole allowed. For electric allowed transition, the equation is dominated by the reciprocal of the electric transition dipole moment.

Crystals, grinding powder, PMMA films, dispersion of MOFs, solution of cages and SOFs were commonly employed in published research for sample fabrication of PCNMs in CD and CPL testing. The detection of CD and CPL is more complex when samples are in the crystalline state, and the presence of linear dichroism (LD) and linearly polarized light emission may lead to potential artifacts in CD and CPL measurements,[5] respectively.

For CD measurement of PCNMs, samples could be recorded at different positions and directions with different angles (0°, 90°, 180°, and 270°) to check and eliminate the LD.[36]

The potential artifacts could be excluded by LD according to previous reports, and the observed CD ($\mathrm{CD_{app}}$) is shown in eqn (8):[37,38]

$$\mathrm{CD_{app}} = \mathrm{CD_{true}} + \mathrm{LD}\cos 2\beta_0 \sin\kappa + 1/6[\mathrm{CB\,LD\,LB} - \mathrm{CDLB}^2 + (1/2\ln 10)^2(\mathrm{CD}^3 + \mathrm{CD\,LD}^2)] \tag{8}$$

where $\mathrm{CD_{app}}$ represents the observed CD signal, $\mathrm{CD_{true}}$ denotes the true CD signal, and LD represents the LD signal, which could be obtained during CD measurement experiments. κ is the static birefringence of the modulator oriented at the angle β_0 to the axis system of the induced birefringence. LB and CB represent the linear and circular birefringence, respectively.

Since the term in square brackets in eqn (8) contains high products of small terms LB and CB, the influence of these terms can be assumed to be negligible compared to the second term. The factor $\cos 2\beta_0 \sin\kappa$ is approximately 0.02 in a CD spectrometer equipped with a photoelastic modulator (PEM). Therefore, eqn (8) can be approximately written as eqn (9):

$$\mathrm{CD_{true}} = \mathrm{CD_{app}} - \mathrm{LD} \times 0.02 \tag{9}$$

This is the semi-empirical equation of true CD signals.

For CPL measurements of PCNMs, the uniformity of these samples is of great importance, so it would be better to grind bulk crystals into a fine powder. The sample was put into a quartz cuvette perpendicular to the test direction, and then was rotated and flipped around after one measurement. The sample is kept under light excitation at an incident angle of 0°/180°.[39] In addition, true CPL signals for optically anisotropic samples can be obtained by the reflective light pathway. The sample is kept under light excitation at an incident angle of 45°,[40] and the angle between the excitation light and the detector is 90°. This approach can also be used with linearly polarized stimulation, such as a laser beam. Any polarization in the *xy* plane might be minimized by aligning the beam direction at 90° and orienting the linear polarization parallel to the emission detection direction.[41] Moreover, to provide solid evidence of CPL, micro-area CPL properties of single crystals could be measured using a home-made experimental setup with a quarter-wave ($\lambda/4$) plate and

Published on 24 Disemba 2021. Downloaded on 8/6/2024 3:24:02 PM.

Table 1 The reported g_{lum} for CPL-active PCNMs derived from direct synthesis, chirality induction or adaption, and symmetry breaking pathways

Chirality origin and mechanism	Chiral PCNMs		$\|g_{lum}\|$	Measurement conditions	Ref.
Direct synthesis	MOFs	Chiral ZIF-8	5.5×10^{-3}	0.9 wt% in toluene, λ_{ex} = 360 nm	46
		$[Zn_2Cam_2DAP]_n$	3×10^{-3}	Thin films	47
		L-/D-Cd-MOFs	0.012	Solid state, 2 mm quartz cuvette	48
			0.58×10^{-3}	After grinding, λ_{ex} = 360 nm	
			3.73×10^{-3}	Suspension in DMF and ultrasonication	
		P-/M-1	2.3×10^{-3}	In solid state, λ_{ex} = 365 nm	42
		P-/M-2	1×10^{-3}		
	MOCs	$[Eu_4(L1)_6](OTf)_{12}$	0.16	1.16×10^{-6} in MeCN	49
		$[Eu_4(L2)_6](OTf)_{12}$	0.04	1 cm path length quartz cuvette	
		$[Eu_4(L3)_6](OTf)_{12}$	0.03	λ_{ex} = 365 nm	
		(Eu_4L_4)(R/S-BINAPO)$_4$	0.2	2.5×10^{-6} M in chloroform	50
		(Eu_4L_4)(DPEPO)$_4$	0.11	λ_{ex} = 395 nm	
		$3^{R/S}$-Eu-cages	0.05	2×10^{-4} M in CH_3CN, λ_{ex} = 350 nm	51
	POCs	T-FRP1	2.8×10^{-4}	0.1 mM in chloroform λ_{ex} = 360 nm	52
		T-FRP2	3.5×10^{-4}		
Chirality induction or adaption	MOFs	ZIFs ⊃ S420/C6/DCM	$9/3/12 \times 10^{-4}$	In solid state, λ_{ex} = 360/450/450 nm	53
		ZIF ⊃ QDs	$3.2–4.6 \times 10^{-3}$	λ_{ex} = 360 nm	
		ZIF ⊃ UCNPs	0.012	λ_{ex} = 980 nm	
		γCD-MOFs ⊃ RuBPen	0.015	In the solid state, λ_{ex} = 450 nm	36
		γCD-MOFs ⊃ ACQ molecule	0.011	λ_{ex} = 450 nm	
		γCD-MOFs ⊃ AIEgen	2×10^{-3}	λ_{ex} = 300 nm	
		P-/M-TbBTC	2.1×10^{-3}	Powder samples, λ_{ex} = 290 nm	43
		P-/M-TbBTC ⊃ DSM	2.5×10^{-3}	λ_{ex} = 514 nm	
		L-/D-MOFs	1.5×10^{-3}	In the solid state, λ_{ex} = 370 nm	54
		L-/D-MOFs ⊃ FS	$1.8/3.4 \times 10^{-3}$	λ_{ex} = 450/370 nm	
		L-/D-MOFs ⊃ RB	$5.2/7.5 \times 10^{-3}$	λ_{ex} = 520/370 nm	
		L-/D-MOFs ⊃ R6G	$6.9/11 \times 10^{-3}$	λ_{ex} = 500/370 nm	
		L-/D-MOFs ⊃ AR	$2.1/3.5 \times 10^{-3}$	λ_{ex} = 520/370 nm	
		L-/D-MOFs ⊃ CBS	1.15×10^{-2}	λ_{ex} = 370 nm	
		La-MOFs ⊃ DAECc, UCNPs	$1.7/7.8 \times 10^{-2}$	Powder samples, λ_{ex} = 360/980 nm	55
			$2.2/6.8 \times 10^{-2}$	PMMA films, λ_{ex} = 360/980 nm	
	MOCs	Chiral Pd cages ⊃ BODIPY 1	2.4×10^{-2}	In the solid state, KBr	56
		Chiral Pd cages ⊃ BODIPY 2	1.0×10^{-2}	λ_{ex} = 450 nm	
	POCs	Anthracene-based nanotube ⊃ ATP	1.0×10^{-2}	[Cage] = 2.5×10^{-5} M in H_2O, 1.0 equiv. ATP, λ_{ex} = 360 nm	57
		TPE-based cage ⊃ deoxynucleotides		[Cage] = 1.0×10^{-4} M in H_2O, [deoxynucleotides] = 2.5×10^{-4} M in H_2O, λ_{ex} = 350 nm	58
		TPE-based cage ⊃ C_2 (cytosine)	2.5×10^{-4}		
		TPE-based cage ⊃ A_2 (adenine)	2.2×10^{-4}		
		TPE-based cage ⊃ T_2 (thymine)	4.7×10^{-4}		
	SOFs	SOF-1 ⊃ Phe	2.0×10^{-4}	[TPE units] = 5.0×10^{-4} M	59
		SOF-1 ⊃ ATP	1.1×10^{-4}	[CB [8]] = 1.0×10^{-3} M	
		SOF-1 ⊃ ADP	1.3×10^{-4}	L/D-Phe (30.0 equiv.)	
		SOF-1 ⊃ AMP	2.0×10^{-4}	ATP (0.5 equiv.), ADP (0.5 equiv.), AMP (5.0 equiv.) in H_2O, λ_{ex} = 365 nm	
Symmetry breaking	MOFs	Tb-MOFs	3.32×10^{-3}	In the solid state, λ_{ex} = 297 nm	60
		Eu^{3+} doped Tb-MOFs	2.56×10^{-4}		
		RTP-MOFs	2.7×10^{-3}	In the solid state, λ_{ex} = 370 nm	61
	POCs	(6P)-1, (6M)-1	1.1×10^{-3}	0.1 mM in chloroform, λ_{ex} = 340 nm	62
		(4P2M)-2, (2P4M)-2	9.3×10^{-4}		

a linear polarizer.[42,43] The circularly polarized emission light passes through the $\lambda/4$ plate and converts into the linear polarization state, while no change occurs in unpolarized light. The relationships between the rotating angles (0°–360°) of the linear polarizer and maximum emission intensity were recorded, and the fast axis of the $\lambda/4$ wave plate was fixed to +45° or −45° simultaneously. If the polarization directions of +45° linear polarized light and −45° linear polarized light are nearly perpendicular, the authenticity of the CPL signal could be further confirmed.

3. Trigger routes of circularly polarized luminescence in porous crystalline nanomaterials

In order to endow PCNMs with CPL properties, two major moieties should be introduced: a luminescent part and a chiral part. If the precursors are chiral and luminescent, these two parts could be connected *via* coordination or covalent bonds to directly synthesize CPL-active PCNMs. As for the chirality

 This journal is © The Royal Society of Chemistry 2022

Published on 24 Disemba 2021. Downloaded on 8/6/2024 3:24:02 PM.

induction method, the achiral luminophores can be endowed with CPL performance through preloading in a chiral-confined space, which is named the "chiral host–achiral luminescent guest" pathway. Additionally, CPL-active PCNMs can be constructed by exclusively achiral precursors, and symmetry breaking during the formation process results in the formation of chiral nanomaterials. In the following section, we will discuss these typical CPL-active PCNMs using some representative examples.

3.1 Direct synthesis of CPL-active porous crystalline nanomaterials

Up to now, nanoscale MOFs, MOCs, and POCs have been representative porous crystalline assemblies to produce CPL properties. MOFs are fabricated with metal secondary building units and organic ligands through coordination bonds, which possess infinite three-dimensional networks. Although MOCs are also composed of organic linkers and metal ions *via* coordination bonds, they form concrete cages.[44] Moreover, POCs are composed of discrete nanoporous molecules, which are constructed with chiral organic linkers and luminescent molecules through covalent bonds. POCs can remain together as solids by weak intermolecular forces.[45] In these situations, metal ions or ligands could play the roles of luminophores, chiral ligands, and chiral ancillary ligands. Ligands can be introduced into systems through one-pot synthesis or post-synthesis ligand exchange.

Zhao *et al.* reported homochiral zeolitic imidazolate frameworks (ZIF-8) showing circularly polarized luminescence.[46] As illustrated in Fig. 1a, ligand exchange between chiral emitters with functional imidazole groups (R-/S-1) and 2-methylimidazole (Hmim) of ZIF-8 could fabricate mixed-ligand chiral ZIF-8. Owing to the ordered assembly of R-/S-1 on the surface of ZIF-8, the $|g_{lum}|$ value of chiral ZIF-8 showed significant amplification by one order of magnitude compared to chiral emitters (from 7.0×10^{-4} to 5.5×10^{-3}). The molecular conformation was locked after R-/S-1 coordinated with Zn^{2+} ions, suppressing the non-radiative transition of the excited state. Therefore, the luminescence efficiency of chiral ZIF-8 was significantly improved. In addition, the chiral ZIF-8 was applied for enantioselective recognition of α-hydroxycarboxylic acids such as tartaric acid (TA) and mandelic acid (MA) due to chiral binaphthyl and –NH– groups of R-/S-1 (Fig. 1b and c). The α-hydroxycarboxylic acid was able to block the photon-induced electron transfer of R-/S-1, giving an L-/D-TA enantioselectivity factor of 4.9 with R-ZIF-8, and an L-/D-MA enantioselectivity factor of 5.2 with R-ZIF-8. These results demonstrated that self-assembly occurring on the MOF surface could improve CPL performance, including the g_{lum} value and luminescence efficiency. For more convenient CPL application, Chen *et al.* reported liquid-phase epitaxial growth of azapyrene and camphoric acid CPL-active chiral MOF thin films, which were named $[Zn_2Cam_2DAP]_n$.[47] Ligands grew on the hydroxyl-functionalized quartz glass with high orientation. Chiral MOF thin films exhibited CD and CPL properties, and the $|g_{lum}|$ magnitude was 10^{-3}. At the same time, the MOFs had good enantioselective adsorption to L-/D-methyl-lactate. This report offered a new approach to construct CPL-active MOFs.

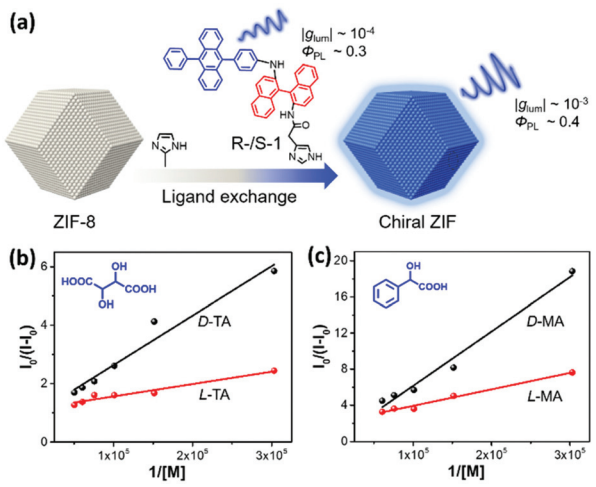

Fig. 1 Direct synthesis of CPL-active MOFs. (a) Amplified CPL and fluorescence efficiency of chiral ZIF-8. (b) Benesi–Hildebrand plot of R-ZIF-8 treated with L-/D-TA (tartaric acid) and (c) L-/D-MA (mandelic acid). Insets show the chemical structures of TA and MA, respectively. Reprinted with permission from ref. 46. Copyright 2019, Wiley-VCH.

Abundant precursors and adjustable coordination morphology in MOFs allowed regulating CPL through tuning the conformation of ligands. Shang *et al.* showed an approach for the fabrication of dual mechano-switched CPL-active MOFs with aggregation-induced-emission chromophores (AIEgens).[48] Achiral AIEgen-tetrakis(4-pyridylphenyl)ethylene (TPyPE) exhibited frame-enhanced luminescence *via* self-assembly with Cd^{2+} ions and chiral Cam. More intriguingly, in condensed L-/D-Cd-MOFs, the AIEgen showed chiroptical properties *via* through-space chirality transfer (Fig. 2a). Due to the dense stacking and fixation of TPyPE, the L-/D-Cd-MOFs showed significant mirror-imaged CPL at 463 nm, while the dissymmetrical factor $|g_{lum}|$ value was up to 0.012 (Fig. 2b). Grinding and ultrasonication enabled stacking and rotation change between AIEgen rotors and frameworks (Fig. 2c). In the as-prepared MOFs, the phenyl rings of TPyPE were orderly oriented and the dihedral angle between the adjacent two phenyl rings was 29.08°. After grinding the L-/D-Cd-MOFs, TPyPE became more tightly arranged, resulting in a smaller dihedral angle (<30°). L-/D-Cd-MOF crystals emitted at 512 nm with a red shift. When the ground powder was suspended in DMF for relaxation, the emission recovered to 463 nm. With ultrasonication of MOFs in DMF, the phenyl conformation became more twisted, resulting in a bigger dihedral angle (>30°) with framework release. The crystals showed fluorescence around 452 nm, and the emission color could recover after removing DMF. Therefore, this finding presented a new example for regulating CPL-active MOFs by introducing facile stimuli such as mechanics.

Besides mechano-regulated CPL, Wang *et al.* constructed turn-on CPL-active MOFs and CPL-silent MOCs by tuning the

Published on 24 Disemba 2021. Downloaded on 8/6/2024 3:24:02 PM.

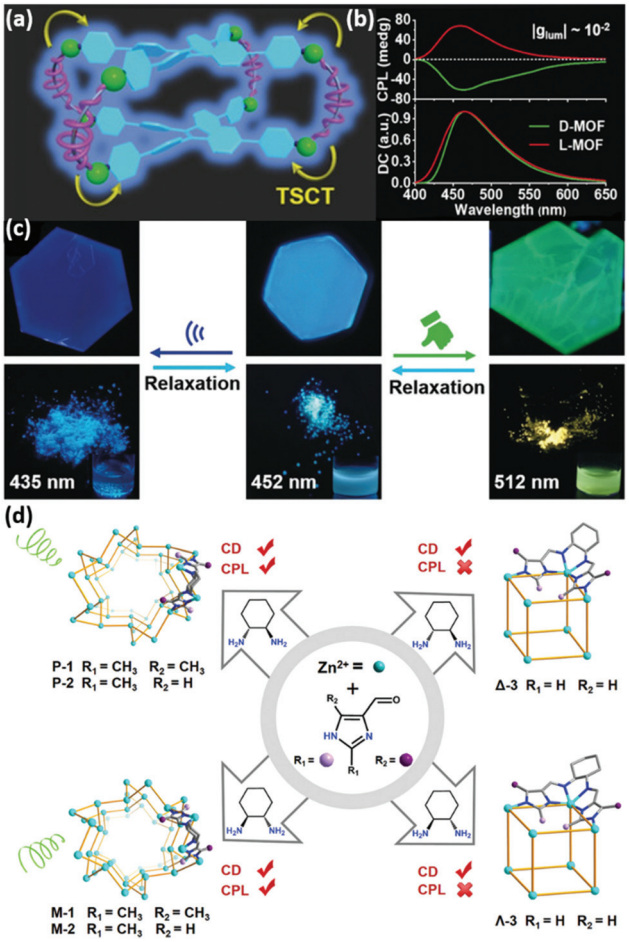

Fig. 2 (a) Illustration of the chiral reticular self-assembly strategy to fabricate optically pure L-/D-Cd-MOFs. (b) Mirror-image CPL spectra of L-/D-Cd-MOFs (red line: L-Cd-MOF, green line: D-Cd-MOF). (c) Fluorescence pictures (excited at 365 nm) of a single crystal (top) and solids (bottom). Reprinted with permission from ref. 48. Copyright 2020, Wiley-VCH. (d) Homochiral Zn-imidazolate 3D MOFs (P-1, M-1, P-2, and M-2) and cubic cages (Λ-3, Λ-3). The MOFs featured CPL activity, while the luminescent chiral cages were CPL-silent. Reprinted with permission from ref. 42. Copyright 2021, Wiley-VCH.

conformations of ligands (Fig. 2d).[42] Homochiral MOFs or MOCs were self-assembled by imidazole derivatives, Zn^{2+}, and chiral 1R-2R-/1S-2S-DCH (1,2-diaminocyclohexane). The 2-methyl group on the imidazole group played an important role in constructing framework structures of P-1, M-1, P-2, and M-2. The whole DCH participated in charge transfer within the imidazolyl groups, which would probably produce excited state chirality to realize CPL activity. The dissymmetry factors of P-1 and M-1 at 520 nm were $\pm 2.3 \times 10^{-3}$. Supramolecular chirality yielded by extended trifold coordination helical chains, which were formed by Zn^{II} binding with the imidazolyl groups in MOFs, can be the reason for the improvement of CPL performance. MOCs Λ-3, Δ-3 were obtained using imidazole-4-carboxaldehyde in the absence of a 2-methyl substituent under the same conditions. The isolated cage structure with limited supramolecular chirality was unable to boost CPL activity.

In addition to the direct synthesis of CPL-active MOFs, MOCs and POCs were also endowed with CPL performance at the nanoscale by combining luminescent and chiral linkers.[51] Yeung *et al.* precisely tuned three europium (Eu) tetrahedral cages through designing three similar chiral ligands with different point chirality.[49] The position of point chirality, especially the distance between metal and chiral centers, played a decisive role in chirality transfer. In this work, the ligand with a highly stereoselective conformation self-assembled into more enantiomeric chiral Eu cages $[Eu_4(\mathbf{L1})_6](OTf)_{12}$. These cages exhibited high luminescence efficiency and relatively better CPL performance ($|g_{lum}|$ up to 0.16). The other two ligands with loose point chirality led to different Eu tetrahedral cages $[Eu_4(\mathbf{L2})_6](OTf)_{12}$ and $[Eu_4(\mathbf{L3})_6](OTf)_{12}$ (**L1**, **L2**, and **L3** are different chiral ligands and OTf is an achiral ligand). Owing to the co-exciting isomer mixtures of ΛΛΛΛ and ΔΔΔΔ-twisted conformations, CPL intensities were weaker. These results indicated that slight changes of conformations have a significant effect on CPL activity.

Moreover, Zhou *et al.* reported the enantiopure europium tetrahedral $(Eu_4L_4)(R/S\text{-BINAPO})_4$ cages *via* chiral auxiliary ligand BINAPO induction.[50] Hydrogen bonds between **L** and BINAPO at each Eu(III) vertex played an important role in chiral induction and stabilization in the homochiral structure. As shown in Fig. 3a, each Eu center was chelated with three achiral ligands **L** and one chiral auxiliary ligand BINAPO. Thus, three β-diketonate units from the **L** ligand formed a left-handed or right-handed helical clamp, giving rise to a distorted geometry. $(Eu_4L_4)(R/S\text{-BINAPO})_4$ cages exhibited significant luminescence with a quantum yield of 81% in solution, and had considerable CPL signals (the $|g_{lum}|$ value at 592 nm was 0.2). Due to the rigid ligand and strong mechanical coupling in MOCs, after replacing chiral auxiliary ligands R-/S-BINAPO by an achiral analogue DPEPO, $(Eu_4L_4)(DPEPO)_4$ MOCs retained chiral memory with a $|g_{lum}|$ value of 0.11 at 592 nm and retained a luminescence efficiency of 68%. Therefore, this demonstrated that the chiral information on the Eu cages was stable. It is worth mentioning that the Eu cages had high g_{lum} inherited by the chiral lanthanide complex advantages[63] and high luminescence efficiency.

Introducing chirality into molecular polyhedra is also a feasible way to obtain CPL-active PCNMs. Two classes of chiral truncated face-rotating polyhedra (T-FRP) were synthesized using chiral diaminocyclohexane (CHDA) and a pentaphenylpyrrole derivative (PPAP) in different solutions (trimethylbenzene, TMB and 1,2-dichloroethane, DCE) (Fig. 3b).[52] Pentaphenylpyrrole (PPP) is a typical AIEgen,[64–66] and restricting the phenyl flipping of PPAP faces could generate P/M chirality and enhance the luminescence performance. T-FRP 1 and T-FRP 2 showed a strong emission peak at 440 nm in chloroform (QY = 33.8% and 35.4%, respectively) in contrast to weak blue emission in the solution of PPAP (QY = 5.5%). Additionally, T-FRP 1 and 2 with a P or M configuration exhibited mirror-image CD signals, confirming induced chirality in solution. The mirror-image CPL signals were observed at 450 nm in chloroform, and the g_{lum} values were $\pm 2.8 \times 10^{-4}$

This journal is © The Royal Society of Chemistry 2022

Published on 24 Disemba 2021. Downloaded on 8/6/2024 3:24:02 PM.

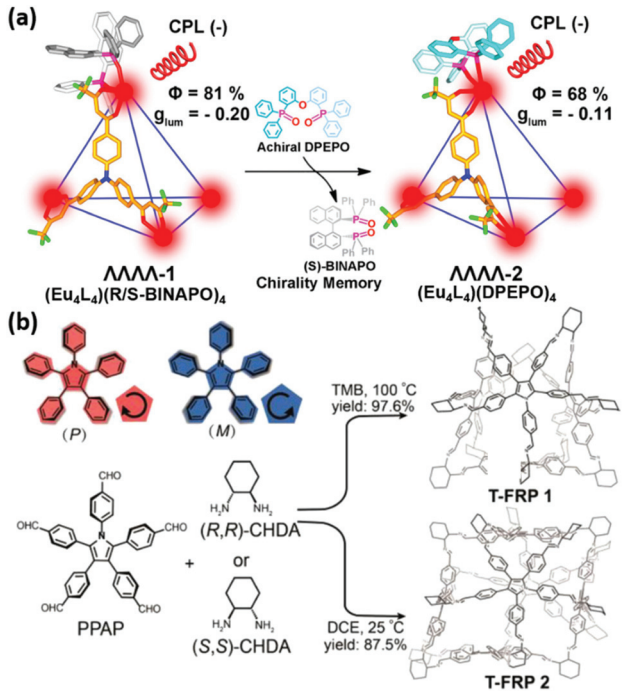

Fig. 3 Direct synthesis of CPL-active cages. (a) Enantiopure Eu-cages were induced by chiral auxiliary ligands R/S-BINAPO. The chiral memory could be retained after R/S-BINAPO was replaced by the achiral ligand DPEPO. Reprinted with permission from ref. 50. Copyright 2019, American Chemical Society. (b) PPP can exhibit clockwise or anticlockwise patterns by restricting propeller-like configurations of phenyl rings (upper left). Scheme of the construction of chiral truncated T-FRP using PPAP as the face and chiral CHDA as vertices in TMB and DCE. Reprinted with permission from ref. 52. Copyright 2020, American Chemical Society.

and $\pm 3.5 \times 10^{-4}$ for T-FRP 1 and T-FRP 2, respectively, which were comparable to those of organic molecules.[35] However, the g_{lum} factor was relatively lower than those of assembled systems, and the POCs were unstable under air, which limited their further applications.

3.2 Chiral induction in CPL-active porous crystalline nanomaterials

Introducing achiral guest emitters into host chiral matrices endows achiral emitters with CPL activity. The non-covalent interaction between the chiral host and the achiral guest is of great importance in chiral induction. Besides non-covalent interactions, a chiral confined microenvironment can also endow achiral emitters with CPL activity by host–guest interactions. Chiral MOFs, which have numerous nanosized chiral helical channels, are appropriate chiral hosts to confine achiral chromophores. In this case, the size matches between the chiral cavities and achiral guests, interactions between the host and guest, and energy levels between the host MOFs and guest should be taken into consideration. Moreover, inducing adaptive chirality of an achiral luminescent host with chiral guests is another strategy to fabricate CPL-active PCNMs. MOCs, POCs, and SOFs are versatile host matrices to form chiral host–guest complexes *via* efficient through-space chirality transfer.[67]

Zhao *et al.* reported facile and general approaches for constructing full-color and white-color solid-state CPL-active ZIFs by loading emitters (Fig. 4a).[53] Chiral ZIFs were synthesized by a mix-ligand coassembly method using Zn^{2+}, chiral histidine, and Hmim (2-methylimidazole). Organic luminophores, quantum dots, and upconversion nanoparticles (UCNPs) were successfully loaded in the chiral ZIFs in their *in situ* synthesis process with high luminescence efficiency and endowed with CPL activity. In addition, size-matched dyes were encapsulated into the cavities of chiral ZIFs, and the induced CPL followed the chirality of ZIFs, while quantum dots with larger size were distributed in the gaps of ZIFs, and induced by the outside chirality of cages, resulting in inverted CPL.[68,69] UCNPs were dispersed in the skeleton of chiral ZIFs, showing excellent upconversion CPL (UC-CPL, g_{lum} values were $\pm 1.2 \times 10^{-2}$) with excitation at 980 nm. The mechanism of directions of induced chirality in chiral MOFs is still needed to investigate.

Besides ZIFs, γCD-MOFs self-assembled by γCD and K^+ were utilized as chiral hosts to encapsulate organic luminophores (Fig. 4b).[36] γCD-MOFs were formed by six γCD faces, leading to chiral cubic voids. The size match effect of CPL induction was thoroughly investigated. When the luminescent dye was much smaller than the γCD-MOF cubic void while

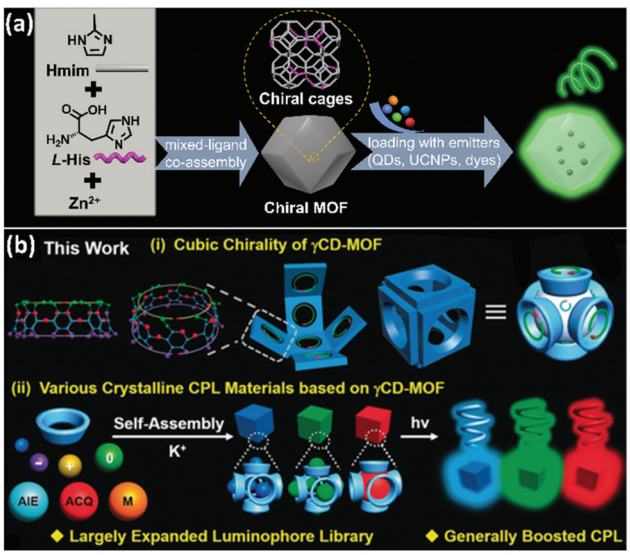

Fig. 4 CPL generation and regulation of luminescent guests induced by the chiral confined space in chiral MOFs. (a) Chiral MOFs synthesized by coordinating 2-methylimidazole (Hmim) and chiral histidine with Zn^{2+}. CPL-active MOFs prepared by loading emitter guests, such as lanthanide-doped upconversion nanoparticles (UCNPs), quantum dots, and organic dyes. Reprinted with permission from ref. 53. Copyright 2020 Tonghan Zhao *et al.* Exclusive Licensee Science and Technology Review Publishing House. Distributed under a Creative Commons Attribution License (CC BY 4.0). The website is as follows: https://creativecommons.org/licenses/by/4.0/. (b) Description of the cubic chirality of γCD-MOFs and CPL-active crystalline materials based on the achiral emitters incorporated into γCD-MOFs. Reprinted with permission from ref. 36. Copyright 2020, Wiley-VCH.

Published on 24 Disemba 2021. Downloaded on 8/6/2024 3:24:02 PM.

being larger than the γCD void, the dye cannot be well constricted in the γCD-MOFs, resulting in uncontrollable CPL signals. While the luminescent guest matched well with the γCD-MOF cubic void or γCD-MOF void, each guest was well confined in the space of the chiral cubic void or the void of γCD, resulting in a determined negative CPL signal ($|g_{lum}|$ value could be up to 0.015). Moreover, besides segregated single AIEgen, ACQ molecules could also be integrated into γCD-MOFs with an induced negative CPL signal, indicating that γCD-MOFs are excellent materials to restrict intramolecular rotation and avoid ACQ. This work provides a deep understanding of induced excited state chirality and the experience of achieving highly efficient crystalline CPL materials.

Chiral lanthanide MOFs were found to be another chiral host to induce CPL activity of guest emitters.[43] Achiral stilbazolium dye (DSM) was incorporated into homochiral MOFs P-(+)/M-(−)-TbBTC. DSM molecules were confined in the chiral space of MOFs and solidified by dangling water molecules within the chiral channel. The CPL of the dye could be observed around 514 nm with a $|g_{lum}|$ of 10^{-3}. By modifying the loading amount of DSM in the TbBTC, color tuning emission from green to red could be observed *via* energy transfer from Tb^{3+} to the encapsulated DSM.

As for chiral cages, Cui's group constructed chiral Pd cages functionalized with crown ether and methoxymethyl groups in the inner surfaces.[56] Chiral hosts encapsulated anionic achiral BODIPY dyes to form stable host–guest systems *via* cation–anion interactions, host–guest interactions and metal-coordination. The host–guest composites manipulated CPL in both solid and solution states with maximum $|g_{lum}|$ values of 2.4×10^{-2}. This work put forward chiral metal–organic cages as a novel platform for host matrices. The chiral perturbation affected achiral dyes and fabricated CPL-active nanomaterials.

In general, the primary CPL is acquired from chiroptical luminescent materials excited by non-polarized light. However, when using circularly polarized light with the same handedness as the excitation light source, chiral emitters will produce CPL with amplified g_{lum} factors since the circularly polarized excitation will significantly enhance the circular polarization of the CPL performance.[70,71] By utilizing energy transfer from a chiral donor to an achiral luminescent acceptor, the chiral donor may generate circularly polarized light to further excite the acceptor.[72] The approach could be regarded as a virtual process of circularly polarized excitation generated by donors, enabling a better CPL performance with larger g_{lum} factors in many molecular assemblies.[73–75] Zhang *et al.* introduced this approach into chiral MOF systems.[54] The enantiomeric pairs of crystalline L-/D-MOFs with helical nanosized channels (1.2 nm) were employed as chiral hosts. Luminescent dyes attached to the inner surface of pores *via* H-bonds and C–H···π interactions, and hence inherited the helicity of L-/D-MOFs (Fig. 5a). Tunable blue to red and white-color emissions with a quantum yield of 30% could be obtained by loading different varieties of dyes. In addition, owing to fluorescence resonance energy transfer (FRET) between L-/D-MOFs and dyes, L-/D-MOF single dye (FS, RB, R6G, AR, and CBS) composites exhibited significantly amplified mirror-image CPL, and the maximum increase was up to tenfold (g_{lum} values were $\pm 1.15 \times 10^{-2}$) compared with direct excitation dyes without energy transfer. In the FRET process, the dipole moment of the helical host interacted with the dyes resulting in dipole–dipole interactions, which can be one of the desirable approaches to amplify the g_{lum} factor in PCNMs.[76]

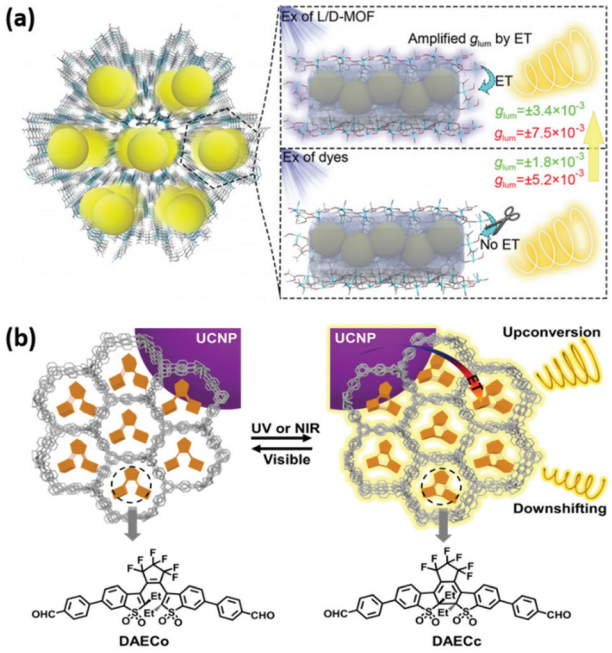

Fig. 5 Energy-transfer-amplified CPL in chiral MOF composite systems. (a) Organic dyes (FS, RB, R6G, AR, and CBS) loaded in the helical channels of enantiomeric MOFs through host–guest interactions with enlarged CPL activities because of FRET from chiral MOF hosts to achiral guests. Reprinted with permission from ref. 54. Copyright 2020, Wiley-VCH. (b) Optically responsive chiral La-MOFs achieved upconversion and downshifting of circularly polarized luminescence switches. Reprinted with permission from ref. 55. Copyright 2021, Wiley-VCH.

Zhao *et al.* have investigated dual upconversion (UC) and downshifting (DS) CPL switches in chiral lanthanide MOFs (La-MOFs), which were fabricated by loading UCNPs and a luminescent diarylethene derivative (DAEC) (Fig. 5b).[55] Reversible photoisomerization from open-ring DAEC (DAECo) to close-ring DAEC (DAECc) was driven by UV light, which was emitted from UCNPs excited by high-power NIR light. It should be noted that DAECc showed higher luminescence efficiency in La-MOFs in contrast to powders, because La-MOFs behaved similarly to a solvent in suppressing serious aggregation. Owing to chirality transfer from the chiral confined skeleton of La-MOFs to DAEC and UCNPs, both UC-CPL and DS-CPL were acquired under UV and NIR light excitation. It was impressive that DAECc showed more excellent UC-CPL (the g_{lum} value was 7.8×10^{-2}) when excited with NIR light in comparison with DS-CPL (g_{lum} value was 1.7×10^{-2}) excited with UV light. Therefore, the enlarged CPL was achieved by energy transfer from inorganic UCNPs to organic systems.

This journal is © The Royal Society of Chemistry 2022

Published on 24 Disemba 2021. Downloaded on 8/6/2024 3:24:02 PM.

Excited-state energy with circular polarization properties of UCNPs transferred to the excited state of DAECc. This strategy is desirable for constructing highly efficient responsive CPL-active PCNMs. In addition, under the irradiation of visible 465 nm light, DAECc could change to colorless DAECo in La-MOFs, resulting in off-state luminescence and CPL. The on–off states of CPL can be experienced several times, suggesting outstanding reversibility and fatigue resistance. Based on these results, a chiroptical logic circuit was constructed with UV, visible, and NIR light as inputs, and with 2D information containing fluorescence and circular polarization as outputs.

The adaptive chirality of an achiral host is defined as a rotational conformational transformation, including cages and macrocycles. Adaptive chirality has applications for chiral recognition of peptides, amino acids, DNA, and deoxynucleotides in water.[77] Cao's group is committed to this field and has presented many excellent reports recently. Cheng *et al.* constructed achiral tetraphenylethylene (TPE)-based octacationic cages bonding with enantiopure deoxynucleotides.[58] In this case, chirality transfer from hydrogen-bonded dimerization of deoxynucleotides to achiral cages occurred. TPE-based cages exhibited adaptive chirality with homo-directional rotation of two TPE units, resulting in CD and CPL signals. Recently, Nian *et al.* reported CPL-active nanotubes in water.[57] Anthracene-based tetracationic nanotubes showed adaptive chirality with P (for UTP and CTP)/M (for ATP and GTP) conformational chirality that originated from adaptive chiral recognition of nucleoside triphosphates. Moreover, a high concentration (0.5–4.0 mM) of the nanotube ⊃ ATP composites formed P-twisted dimeric stacking between two anthracene rings, implying anthracene excimer emission and strong CPL intensity in water (the g_{lum} value was 1.0×10^{-2} at 550 nm). Other high concentration composites (nanotube ⊃ GTP, UTP, CTP) were CPL silent because of high repulsive force and the ACQ effect. Therefore, the hierarchical two-level supramolecular adaptive chirality of host–guest complexes could be a good tool to distinguish biomolecules with tiny structural differences through CD and CPL signals.

In addition to the adaptive chirality systems mentioned above, Li *et al.* reported an achiral cucurbit [8]-based (CB[8]) SOF with coumarin and dynamic rotational conformation of TPE units (SOF-1), which exhibited adaptive chirality induced by L-/D-phenylalanine (Phe) in water (Fig. 6a).[59] Hetero-dimerization of partial CB[8] with coumarin units and Phe within the skeleton of SOF-1 resulted in effective through-space chirality transfer from Phe to TPE units. Mirror-image CD and CPL signals were observed for the chiral SOF-1 complexes, and the g_{lum} values were -2.0×10^{-4} for P-SOF-1 ⊃ D-Phe and -1.3×10^{-4} for M-SOF-1 ⊃ L-Phe, respectively. ATP, ADP, and AMP with negative charges and D-type chirality were bound to the positively charged cavities of P-SOF-1 *via* electrostatic interactions, showing a negative Cotton effect and right-handed CPL signals (g_{lum} values were -1.1×10^{-4}, -1.3×10^{-4}, and -2.0×10^{-4} for ATP, ADP, and AMP, respectively). In this case, SOFs were indispensable spaces for chirality transfer and intermolecular hetero-dimerization.

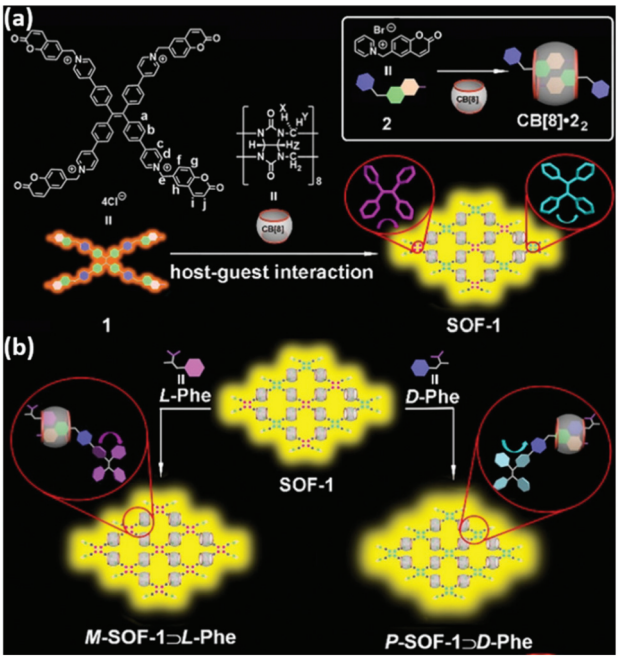

Fig. 6 Adaptive chirality of an achiral host for chirality induction by a chiral guest. (a) CB[8] and TPE derivative (**1**) formed SOF-1. Inset: SOF formation mechanism: the homodimerization between two guest molecules **2** and a CB[8] host. (b) Adaptive chirality of SOF-1 induced by L-/D-Phe. Reprinted with permission from ref. 59. Copyright 2021, Wiley-VCH.

3.3 Symmetry breaking in luminescent porous crystalline nanomaterials

In the above approaches, chiral components, either in the PCNM form or as induced reagents, are indispensable to generate CPL performance in PCNMs. However, not only chiral precursors but also exclusively achiral components can fabricate chiral PCNMs. Spontaneous symmetry breaking results in nanoscale chirality in these systems.

For the formation of chiral MOFs by achiral precursors, when the first coordination polymer nucleated, it had an induction effect on the next, so that the whole systems were inclined to one direction.[78] Yang *et al.* reported CPL-active symmetry breaking Ln-MOFs (Ln = Eu^{3+} and Tb^{3+} ions) with optical waveguide properties using a solvothermal method.[79] Ln^{3+} ions were connected together to generate 1D inorganic helical chains and 1D chains linked with each other *via* phenyl groups of 1,3,5-benzenetricarboxylic acid ligands, showing a 3D framework structure. Under excitation light, emission of 1D microrods propagated to the tip, exhibiting optical-waveguide properties. Tb-MOFs showed negative CPL signals with a g_{lum} value of -3.32×10^{-3} and Eu^{3+} doped Tb-MOFs with a g_{lum} value of -2.56×10^{-4}. Therefore, exclusively achiral components could form CPL-active MOFs.

MOFs also broadened the horizons of phosphorescent materials. Du *et al.* illustrated CPL-active MOFs showing room-temperature phosphorescence (RTP) without precious metals and chiral components; the structure of RTP-MOFs is shown

Published on 24 Disemba 2021. Downloaded on 8/6/2024 3:24:02 PM.

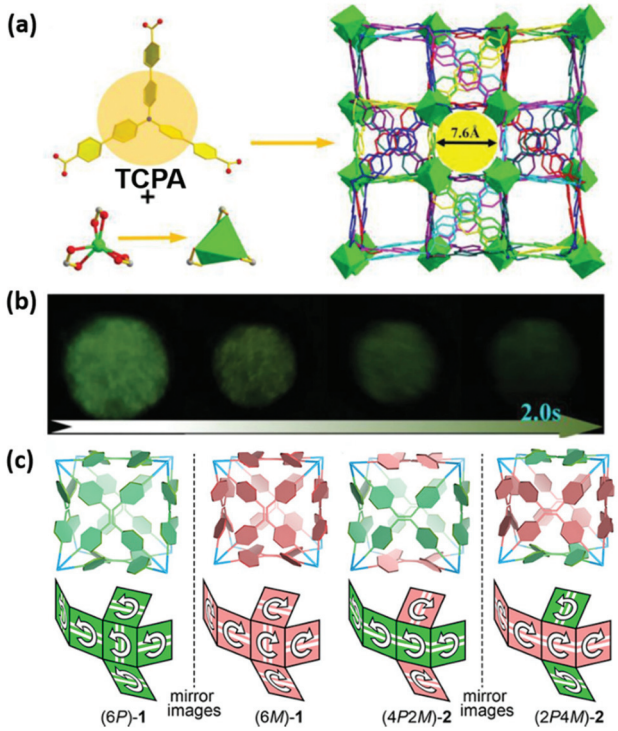

Fig. 7 (a) Fan-shaped Cd^{2+} coordinated with three carboxylate groups on three tridentate ligands TCPA and a 3D interpenetrated framework. (b) Luminescence photographs of RTP MOFs after the removal of 365 nm UV irradiation. Reprinted with permission from ref. 61. Copyright 2020, Wiley-VCH. (c) Diagram of four kinds of TPE-based chiral cubes, homodirectional cubes (6P)-1 and (6M)-1, and the heterodirectional cubes (4P2M)-2 and (2P4M)-2. Reprinted with permission from ref. 62. Copyright 2017, American Chemical Society.

in Fig. 7a.[61] Breaking symmetric MOFs were formed by Cd^{2+} ions and tris(4′-carboxy-1,1′-biphenyl)amine (TCPA). The $[Cd(COO)_3]^-$ coordination unit possessed a threefold rotational symmetry and took a Λ conformation with a fan-like shape. Fluorescence around 475 nm and long-lived RTP (1.22 s) around 525 nm of MOFs were detected upon excitation at 370 nm (Fig. 7b). The RTP was probably caused by the restricted motions of TCPA and repressed nonradiative emission of excitons.[60,80,81] The homochiral structure of MOFs triggered a negative CPL signal with a g_{lum} value of -2.7×10^{-3} at 480 nm. Owing to diminishing the ACQ effect *via* rigid MOF skeletons, tuneable emission was acquired by encapsulation of ACQ dyes, including coumarin 6, acriflavine, and rhodamine B (RhB). White light emission was obtained by modulating the amount of RhB, and a simple LED was fabricated by coating MOFs ⊃ RhB on the surface of a UV LED.

These results indicated that MOFs paved a new way for chiral fluorescent/phosphorescent hybrid systems.

In another case, symmetry breaking during self-assembly could also construct chiral cage compounds. Cao's group fabricated chiral face-rotating cubes (FRCs) formed by TPE and triamine.[62] There were dynamic covalent interactions between TPE derivative faces and triamine vertices in cages. The

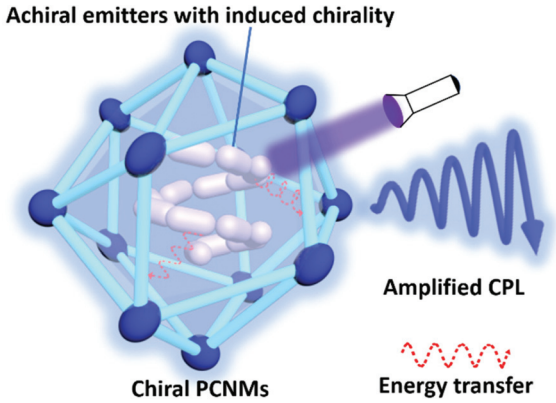

Scheme 2 Achiral emitters distributed in the channels or dispersed in the skeleton of PCNMs, and then obtained induced chirality. The PCNMs had intrinsic CPL performance. When achiral emitters were directly excited, there was energy transfer from donors to acceptors. (Red dotted arrow: energy transfer.)

covalent interactions restricted the intramolecular flipping of phenyl rings in TPE, which presented regular orientational P or M rotational configurations. The resulting product was a mixture, as shown in Fig. 7c. Two pairs of enantiomeric POCs were separated by HPLC. The homodirectional TPE cages (6P)-1 and (6M)-1, and the heterodirectional (4P2M)-2 and (2P4M)-2 showed enhanced fluorescence and chiroptical properties. CPL emissions were observed around 450 nm in chloroform, with considerable $|g_{lum}| = 1.1 \times 10^{-3}$ for (6P)-1 (+) and (6M)-1 (−), and smaller $|g_{lum}| = 9.3 \times 10^{-4}$ for (4P2M)-2 (+) and (2P4M)-2 (−). Despite fine control of symmetry, breaking POCs is a challenge, and this work is a useful example for constructing chiral cages.

4. Conclusions and perspectives

In conclusion, CPL-active PCNMs have attracted increasing research interest owing to their advantages of large g_{lum} values and high luminescence efficiency. This minireview provides a summary of fabricating and modulating CPL-active PCNMs, including MOFs, MOCs, POCs, and SOFs. Three approaches are discussed: direct synthesis, chiral induction, and symmetry breaking. All these methods introduce chirality at the nanoscale, bringing out chiroptical activities. Additionally, in these systems, the combination of energy transfer and excited state chirality can be one of the most useful approaches for CPL amplification.

Despite many efforts being devoted to developing CPL-active PCNMs, further explorations are still needed. Energy transfer, such as fluorescence resonance energy transfer, is confirmed to be able to amplify the g_{lum} value of CPL in chiral MOF systems. However, the detailed theoretical mechanism still needs thorough investigations. Furthermore, although the g_{lum} values of these systems can reach 10^{-2}, there is still a lot of room for improvement. On the one hand, in the energy

 This journal is © The Royal Society of Chemistry 2022

Published on 24 Disemba 2021. Downloaded on 8/6/2024 3:24:02 PM.

transfer system, it is important to design an energy donor and acceptor. The following features need to be taken into consideration in energy transfer systems: a sufficient overlap of the emission spectrum of the donor and the adsorption peak of the acceptor in RET (radiative energy transfer) and FRET systems, with a short donor–acceptor distance normally less than 10 nm in FRET systems. Chiral and luminescent PCNMs could act as chiral energy acceptors, exhibiting CPL performance. Achiral emitters as energy donors are incorporated into chiral matrices, enabling induced chirality. Subsequently, the circularly polarized emission of the energy donor can further excite the chiral PCNMs, which can be regarded as a virtual process of circularly polarized excitation, boosting the CPL performance of chiral PCNMs compared with the one under direct excitation by unpolarized light.[39,70] An amplified g_{lum} value of PCNMs can be realized (Scheme 2). On the other hand, nanosized ZIFs and cages (POCs and MOCs) may have good dispersibility or solubility, and could be ideal dopants in chiral liquid crystal systems, enabling a large g_{lum} value of PCNMs.

In addition, although chiral induction has been successfully achieved in achiral emitters encapsulated in chiral MOFs, the relationships between the host chirality and induced chirality of the guest have not been clearly explained. The possible reason is the size matching effect between the chiral host and the achiral guest. In-depth experiments and theoretical calculations should be performed. Moreover, chiral cages possess high emission efficiency, good solubility, and stable structures, but it is still a challenge to prepare CPL-active molecular cages (MOCs and POCs). Therefore, expansion of the types of CPL-active cages and further exploration of the structure–property relationship are necessary.

Owing to the outstanding performances of CPL-active PCNMs, we propose some functional applications. On the one hand, CPL-active PCNMs are high-performance solid-state CPL materials for optoelectronic applications, and are a good platform for asymmetric photocatalysis owing to their high surface area and tuneable porosity. Additionally, their flexible structure makes it convenient to construct stimuli-responsive materials, which provide a platform for intelligent response CPL materials.

On the other hand, good solubility of CPL-active PCNMs (such as SOFs and cages) could be used for enantiomer recognition and separation. Therefore, further efforts need to be devoted. We believe that the improvement of CPL-active PCNMs will provide a huge platform for practical applications.

Author contributions

P. F. Duan conceived the idea and supervised the project. A. Y. Zheng wrote the manuscript. P. F. Duan, T. H. Zhao, X. Jin and W. G. Miao revised the review.

Conflicts of interest

There are no conflicts to declare.

Acknowledgements

This work was supported by the Beijing Natural Science Foundation (JQ21003, 2212023), the National Natural Science Foundation of China (21773103, 21802027, 22172041, 91856115 and 52173159), the Strategic Priority Research Program of Chinese Academy of Sciences (XDB36000000) and the Ministry of Science and Technology of the People's Republic of China (2017YFA0206600).

Notes and references

1 E. Yashima, K. Maeda, H. Iida, Y. Furusho and K. Nagai, *Chem. Rev.*, 2009, **109**, 6102–6211.
2 M. Liu, L. Zhang and T. Wang, *Chem. Rev.*, 2015, **115**, 7304–7397.
3 G. Wu, Y. Liu, Z. Yang, N. Katakam, H. Rouh, S. Ahmed, D. Unruh, K. Surowiec and G. Li, *Research*, 2019, **2019**, 6717104.
4 F. S. Richardson and J. P. Riehl, *Chem. Rev.*, 1977, **77**, 773–792.
5 J. P. Riehl and F. S. Richardson, *Chem. Rev.*, 1986, **86**, 1–16.
6 M. Schadt, *Annu. Rev. Mater. Sci.*, 1997, **27**, 305–379.
7 J. F. Sherson, H. Krauter, R. K. Olsson, B. Julsgaard, K. Hammerer, I. Cirac and E. S. Polzik, *Nature*, 2006, **443**, 557–560.
8 C. Wagenknecht, C.-M. Li, A. Reingruber, X.-H. Bao, A. Goebel, Y.-A. Chen, Q. Zhang, K. Chen and J.-W. Pan, *Nat. Photonics*, 2010, **4**, 549–552.
9 H. Zheng, W. Li, W. Li, X. Wang, Z. Tang, S. X.-A. Zhang and Y. Xu, *Adv. Mater.*, 2018, **30**, 1705948.
10 T. Kawasaki, M. Sato, S. Ishiguro, T. Saito, Y. Morishita, I. Sato, H. Nishino, Y. Inoue and K. Soai, *J. Am. Chem. Soc.*, 2005, **127**, 3274–3275.
11 C. He, G. Yang, Y. Kuai, S. Shan, L. Yang, J. Hu, D. Zhang, Q. Zhang and G. Zou, *Nat. Commun.*, 2018, **9**, 5117.
12 H. Zheng, B. Ju, X. Wang, W. Wang, M. Li, Z. Tang, S. X.-A. Zhang and Y. Xu, *Adv. Opt. Mater.*, 2018, **6**, 1801246.
13 F. Song, G. Wei, X. Jiang, F. Li, C. Zhu and Y. Cheng, *Chem. Commun.*, 2013, **49**, 5772–5774.
14 G. Longhi, E. Castiglioni, J. Koshoubu, G. Mazzeo and S. Abbate, *Chirality*, 2016, **28**, 696–707.
15 J. L. Lunkley, D. Shirotani, K. Yamanari, S. Kaizaki and G. Muller, *J. Am. Chem. Soc.*, 2008, **130**, 13814–13815.
16 M. Sugimoto, X. L. Liu, S. Tsunega, E. Nakajima, S. Abe, T. Nakashima, T. Kawai and R. H. Jin, *Chem. – Eur. J.*, 2018, **24**, 6519–6524.
17 H. Tanaka, Y. Inoue and T. Mori, *ChemPhotoChem*, 2018, **2**, 386–402.
18 K. Dhbaibi, L. Favereau, M. Srebro-Hooper, M. Jean, N. Vanthuyne, F. Zinna, B. Jamoussi, L. Di Bari, J. Autschbach and J. Crassous, *Chem. Sci.*, 2018, **9**, 735–742.
19 J. Han, J. You, X. Li, P. Duan and M. Liu, *Adv. Mater.*, 2017, **29**, 1606503.

Published on 24 Disemba 2021. Downloaded on 8/6/2024 3:24:02 PM.

20 D. Yang, P. Duan, L. Zhang and M. Liu, *Nat. Commun.*, 2017, **8**, 15727.
21 B. Han, *Acta Phys.-Chim. Sin.*, 2019, **35**, 1177–1178.
22 M. Zhou, S. Jiang, T. Zhang, Y. Shi, X. Jin and P. Duan, *Prog. Chem.*, 2020, **32**, 361–370.
23 X. Li, W. Hu, Y. Wang, Y. Quan and Y. Cheng, *Chem. Commun.*, 2019, **55**, 5179–5182.
24 X. Li, Q. Li, Y. Wang, Y. Quan, D. Chen and Y. Cheng, *Chem. – Eur. J.*, 2018, **24**, 12607–12612.
25 C. D. Wu, A. Hu, L. Zhang and W. B. Lin, *J. Am. Chem. Soc.*, 2005, **127**, 8940–8941.
26 L. Ma, C. Abney and W. Lin, *Chem. Soc. Rev.*, 2009, **38**, 1248–1256.
27 P. Wu, C. He, J. Wang, X. Peng, X. Li, Y. An and C. Duan, *J. Am. Chem. Soc.*, 2012, **134**, 14991–14999.
28 J. Jiao, C. Tan, Z. Li, Y. Liu, X. Han and Y. Cui, *J. Am. Chem. Soc.*, 2018, **140**, 2251–2259.
29 M. M. Wanderley, C. Wang, C.-D. Wu and W. Lin, *J. Am. Chem. Soc.*, 2012, **134**, 9050–9053.
30 C. Zhu, H. Tang, K. Yang, Y. Fang, K.-Y. Wang, Z. Xiao, X. Wu, Y. Li, J. A. Powell and H.-C. Zhou, *J. Am. Chem. Soc.*, 2021, **143**, 12560–12566.
31 L.-X. He, C.-R. Tian, J.-H. Zhang, W. Xu, B. Peng, S.-M. Xie, M. Zi and L.-M. Yuan, *Electrophoresis*, 2020, **41**, 104–111.
32 X. C. Huang, Y. Y. Lin, J. P. Zhang and X. M. Chen, *Angew. Chem., Int. Ed.*, 2006, **45**, 1557–1559.
33 J. Dong, C. Tan, K. Zhang, Y. Liu, P. J. Low, J. Jiang and Y. Cui, *J. Am. Chem. Soc.*, 2017, **139**, 1554–1564.
34 Y. Lu, H. Zhang, Y. Zhu, P. J. Marriott and H. Wang, *Adv. Funct. Mater.*, 2021, **31**, 2101335.
35 E. M. Sanchez-Carnerero, A. R. Agarrabeitia, F. Moreno, B. L. Maroto, G. Muller, M. J. Ortiz and S. de la Moya, *Chem. – Eur. J.*, 2015, **21**, 13488–13500.
36 L. Hu, K. Li, W. Shang, X. Zhu and M. Liu, *Angew. Chem., Int. Ed.*, 2020, **59**, 4953–4958.
37 A. Davidsson, B. Norden and S. Seth, *Chem. Phys. Lett.*, 1980, **70**, 313–316.
38 A. Ohira, K. Okoshi, M. Fujiki, M. Kunitake, M. Naito and T. Hagihara, *Adv. Mater.*, 2004, **16**, 1645–1650.
39 T. Zhao, J. Han, P. Duan and M. Liu, *Acc. Chem. Res.*, 2020, **53**, 1279–1292.
40 J. E. Field, G. Muller, J. P. Riehl and D. Venkataraman, *J. Am. Chem. Soc.*, 2003, **125**, 11808–11809.
41 H. Tsumatori, T. Nakashima and T. Kawai, *Org. Lett.*, 2010, **12**, 2362–2365.
42 X.-Z. Wang, M.-Y. Sun, Z. Huang, M. Xie, R. Huang, H. Lu, Z. Zhao, X.-P. Zhou and D. Li, *Adv. Opt. Mater.*, 2021, 2002096.
43 M. Zeng, A. Ren, W. Wu, Y. Zhao, C. Zhan and J. Yao, *Chem. Sci.*, 2020, **11**, 9154–9161.
44 M. Pan, K. Wu, J.-H. Zhang and C.-Y. Su, *Coord. Chem. Rev.*, 2019, **378**, 333–349.
45 J.-H. Zhang, S.-M. Xie, M. Zi and L.-M. Yuan, *J. Sep. Sci.*, 2020, **43**, 134–149.
46 T. Zhao, J. Han, X. Jin, Y. Liu, M. Liu and P. Duan, *Angew. Chem., Int. Ed.*, 2019, **58**, 4978–4982.
47 S.-M. Chen, L.-M. Chang, X.-K. Yang, T. Luo, H. Xu, Z.-G. Gu and J. Zhang, *ACS Appl. Mater. Interfaces*, 2019, **11**, 31421–31426.
48 W. Shang, X. Zhu, T. Liang, C. Du, L. Hu, T. Li and M. Liu, *Angew. Chem., Int. Ed.*, 2020, **59**, 12811–12816.
49 C.-T. Yeung, K.-H. Yim, H.-Y. Wong, R. Pal, W.-S. Lo, S.-C. Yan, M. Y.-M. Wong, D. Yufit, D. E. Smiles, L. J. McCormick, S. J. Teat, D. K. Shuh, W.-T. Wong and G.-L. Law, *Nat. Commun.*, 2017, **8**, 1128.
50 Y. Zhou, H. Li, T. Zhu, T. Gao and P. Yan, *J. Am. Chem. Soc.*, 2019, **141**, 19634–19643.
51 Z. Wang, L.-P. Zhou, T.-H. Zhao, L.-X. Cai, X.-Q. Guo, P.-F. Duan and Q.-F. Sun, *Inorg. Chem.*, 2018, **57**, 7982–7992.
52 H. Qu, Z. Huang, X. Dong, X. Wang, X. Tang, Z. Li, W. Gao, H. Liu, R. Huang, Z. Zhao, H. Zhang, L. Yang, Z. Tian and X. Cao, *J. Am. Chem. Soc.*, 2020, **142**, 16223–16228.
53 T. Zhao, X. Jin, M. Zhou, Y. Liu, P. Duan and M. Liu, *Research*, 2020, 6452123.
54 C. Zhang, Z.-P. Yan, X.-Y. Dong, Z. Han, S. Li, T. Fu, Y.-Y. Zhu, Y.-X. Zheng, Y.-Y. Niu and S.-Q. Zang, *Adv. Mater.*, 2020, **32**, 2002914.
55 T. Zhao, J. Han, Y. Shi, J. Zhou and P. Duan, *Adv. Mater.*, 2021, **33**, 2101797.
56 X. Tang, H. Jiang, Y. Si, N. Rampal, W. Gong, C. Cheng, X. Kang, D. Fairen-Jimenez, Y. Cui and Y. Liu, *Chem*, 2021, **7**, 2771–2786.
57 H. Nian, L. Cheng, L. Wang, H. Zhang, P. Wang, Y. Li and L. Cao, *Angew. Chem., Int. Ed.*, 2021, **60**, 15354–15358.
58 L. Cheng, K. Liu, Y. Duan, H. Duan, Y. Li, M. Gao and L. Cao, *CCS Chem.*, 2020, **2**, 2749–2763.
59 Y. Li, Q. Li, X. Miao, C. Qin, D. Chu and L. Cao, *Angew. Chem., Int. Ed.*, 2021, **60**, 6744–6751.
60 M. Baroncini, G. Bergamini and P. Ceroni, *Chem. Commun.*, 2017, **53**, 2081–2093.
61 H.-R. Fu, N. Wang, X.-X. Wu, F.-F. Li, Y. Zhao, L.-F. Ma and M. Du, *Adv. Opt. Mater.*, 2020, **8**, 2000330.
62 H. Qu, Y. Wang, Z. Li, X. Wang, H. Fang, Z. Tian and X. Cao, *J. Am. Chem. Soc.*, 2017, **139**, 18142–18145.
63 H. G. Brittain and F. S. Richardson, *J. Am. Chem. Soc.*, 1976, **98**, 5858–5863.
64 X. Feng, B. Tong, J. Shen, J. Shi, T. Han, L. Chen, J. Zhi, P. Lu, Y. Ma and Y. Dong, *J. Phys. Chem. B*, 2010, **114**, 16731–16736.
65 L. Zhang, K. Liang, L. Dong, P. Yang, Y. Li, X. Feng, J. Zhi, J. Shi, B. Tong and Y. Dong, *New J. Chem.*, 2017, **41**, 8877–8884.
66 Y. Lei, Q. Liu, L. Dong, Z. Cai, J. Shi, J. Zhi, B. Tong and Y. Dong, *Chem. – Eur. J.*, 2018, **24**, 14269–14274.
67 P. Howlader, S. Mondal, S. Ahmed and P. S. Mukherjee, *J. Am. Chem. Soc.*, 2020, **142**, 20968–20972.
68 M. Kodaka, *J. Phys. Chem. Lett.*, 1991, **95**, 2110–2112.
69 M. Kodaka, *J. Am. Chem. Soc.*, 1993, **115**, 3702–3705.
70 I. Z. Steinberg and B. Ehrenberg, *J. Chem. Phys.*, 1974, **61**, 3382–3386.
71 G. L. Hilmes, J. M. Timper and J. P. Riehl, *Inorg. Chem.*, 1985, **24**, 1721–1723.

 This journal is © The Royal Society of Chemistry 2022

72 C. Li, X. Jin, J. Han, T. Zhao and P. Duan, *J. Phys. Chem. Lett.*, 2021, **12**, 8566–8574.
73 L. Ji, Y. Sang, G. Ouyang, D. Yang, P. Duan, Y. Jiang and M. Liu, *Angew. Chem., Int. Ed.*, 2019, **58**, 844–848.
74 J. Wade, J. R. Brandt, D. Reger, F. Zinna, K. Y. Amsharov, N. Jux, D. L. Andrews and M. J. Fuchter, *Angew. Chem., Int. Ed.*, 2021, **60**, 222–227.
75 K. Yao, Y. Shen, Y. Li, X. Li, Y. Quan and Y. Cheng, *J. Phys. Chem. Lett.*, 2021, **12**, 598–603.
76 Y. Yang, R. C. da Costa, M. J. Fuchter and A. J. Campbell, *Nat. Photonics*, 2013, **7**, 634–638.
77 H. Zhang, L. Cheng, H. Nian, J. Du, T. Chen and L. Cao, *Chem. Commun.*, 2021, **57**, 3135–3138.
78 S.-T. Wu, Y.-R. Wu, Q.-Q. Kang, H. Zhang, L.-S. Long, Z. Zheng, R.-B. Huang and L.-S. Zheng, *Angew. Chem., Int. Ed.*, 2007, **46**, 8475–8479.
79 X. Yang, X. Lin, Y. Zhao, Y. S. Zhao and D. Yan, *Angew. Chem., Int. Ed.*, 2017, **56**, 7853–7857.
80 S. Kuno, H. Akeno, H. Ohtani and H. Yuasa, *Phys. Chem. Chem. Phys.*, 2015, **17**, 15989–15995.
81 S. Pan, Z. Chen, X. Zheng, D. Wu, G. Chen, J. Xu, H. Feng and Z. Qian, *J. Phys. Chem. Lett.*, 2018, **9**, 3939–3945.

Published on 24 Disemba 2021. Downloaded on 8/6/2024 3:24:02 PM.